BIOCHEMISTRY
including biophysical chemistry & molecular biology

Article

pubs.acs.org/biochemistry

Structure and Function of the Genomically Encoded Fosfomycin Resistance Enzyme, FosB, from *Staphylococcus aureus*

Matthew K. Thompson,[†] Mary E. Keithly,[‡] Michael C. Goodman,[‡] Neal D. Hammer,[§] Paul D. Cook,[∥] Kevin L. Jagessar,[†] Joel Harp,[⊥] Eric P. Skaar,[§] and Richard N. Armstrong*[,†,‡,⊥]

[†]Department of Biochemistry, Vanderbilt University School of Medicine, Nashville, Tennessee 37232, United States

[‡]Department of Chemistry, Vanderbilt University, Nashville, Tennessee 37235, United States

[§]Department of Pathology, Microbiology and Immunology, Vanderbilt University School of Medicine, Nashville, Tennessee 37235, United States

[∥]Department of Chemistry, Grand Valley State University, Allendale, Michigan 49401, United States

[⊥]Center for Structural Biology, Vanderbilt University, Nashville, Tennessee 37235, United States

Supporting Information

ABSTRACT: The Gram-positive pathogen *Staphylococcus aureus* is a leading cause of global morbidity and mortality. Like many multi-drug-resistant organisms, *S. aureus* contains antibiotic-modifying enzymes that facilitate resistance to a multitude of antimicrobial compounds. FosB is a Mn^{2+}-dependent fosfomycin-inactivating enzyme found in *S. aureus* that catalyzes nucleophilic addition of either L-cysteine (L-Cys) or bacillithiol (BSH) to the antibiotic, resulting in a modified compound with no bactericidal properties. The three-dimensional X-ray crystal structure of FosB from *S. aureus* ($FosB^{Sa}$) has been determined to a resolution of 1.15 Å. Cocrystallization of $FosB^{Sa}$ with either L-Cys or BSH results in a disulfide bond between the exogenous thiol and the active site Cys9 of the enzyme. An analysis of the structures suggests that a highly conserved loop region of the FosB enzymes must change conformation to bind fosfomycin. While two crystals of $FosB^{Sa}$ contain Zn^{2+} in the active site, kinetic analyses of $FosB^{Sa}$ indicated that the enzyme is inhibited by Zn^{2+} for L-Cys transferase activity and only marginally active for BSH transferase activity. Fosfomycin-treated disk diffusion assays involving *S. aureus* Newman and the USA300 JE2 methicillin-resistant *S. aureus* demonstrate a marked increase in the sensitivity of the organism to the antibiotic in either the BSH or FosB null strains, indicating that both are required for survival of the organism in the presence of the antibiotic. This work identifies FosB as a primary fosfomycin-modifying pathway of *S. aureus* and establishes the enzyme as a potential therapeutic target for increased efficacy of fosfomycin against the pathogen.

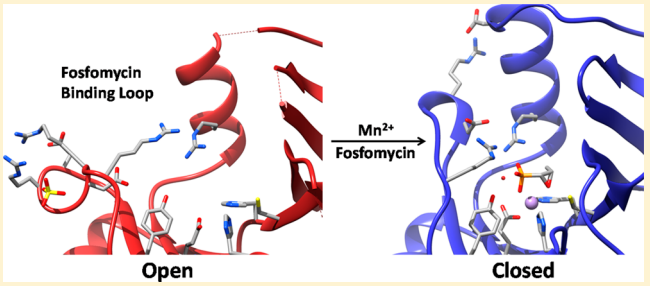

The Gram-positive pathogen *Staphylococcus aureus* is a leading cause of global morbidity and mortality.[1,2] This organism innocuously colonizes the anterior nares of nearly one-third of the world's population and is commonly associated with commensal colonization of the skin.[3,4] *S. aureus* poses a serious risk to public health because of its prevalence as a commensal organism, its ability to cause a multitude of diseases, and the increasing incidence of antibiotic-resistant strains like methicillin-resistant *S. aureus* (MRSA). Herein, we characterize the resistance mechanism of MRSA to the antibiotic fosfomycin.

Fosfomycin is a safe, broad-spectrum antibiotic that is effective against both Gram-negative and Gram-positive bacteria. It is most often prescribed for the treatment of urinary tract and gastrointestinal infections.[5−8] Fosfomycin has few human side effects and is excreted from the body in its unmetabolized, active form. Therefore, it can be administered in a single 3 g dose in the clinical setting. Fosfomycin inhibits cell wall biogenesis by covalently binding to an active site cysteine of MurA, the enzyme responsible for the first committed step in peptidoglycan biosynthesis, a historically important target for antimicrobial agents. A significant disadvantage of the effectiveness of fosfomycin has been the emergence of pathogens that contain fosfomycin-modifying enzymes.

FosB, a Mn^{2+}-dependent fosfomycin-inactivating enzyme found in Gram-positive organisms such as *S. aureus*, is one of three related enzymes (FosA, FosB, and FosX) that confer resistance to the antibiotic.[9−16] The enzyme catalyzes nucleophilic addition of bacillithiol (BSH), a unique low-molecular weight (LMW) thiol native to Gram-positive bacteria,[17] to C1 of fosfomycin, resulting in a modified, inactive

Received: November 26, 2013
Revised: January 8, 2014
Published: January 8, 2014

   dx.doi.org/10.1021/bi4015852 | *Biochemistry* 2014, 53, 755−765

compound (Figure 1). FosB was originally characterized as a Mg^{2+}-dependent L-cysteine (L-Cys) transferase.[18] However, the

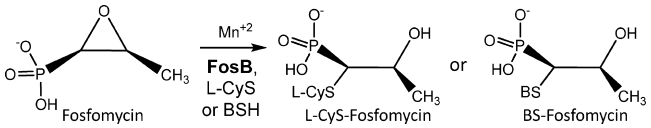

Figure 1. Reaction catalyzed by the fosfomycin resistance protein, FosB. FosB is a thiol-dependent fosfomycin-inactivating enzyme found in *S. aureus* that catalyzes nucleophilic addition of either L-cysteine or bacillithiol to C1 of the antibiotic, resulting in a modified compound with no bactericidal properties.

synthesis of BSH has allowed further investigation into the thiol preference of the FosB enzymes, and kinetic analyses indicate a preference of the FosB enzymes for BSH over L-Cys as the cosubstrate for nucleophilic addition to the antibiotic.[19]

BSH was first identified in 2009 and isolated from *S. aureus* and *Deinococcus radiodurans* (Figure 2).[20] It is the α-anomeric

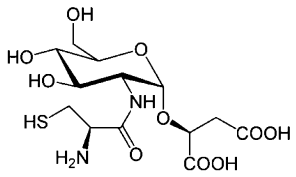

Figure 2. Structure of bacillithiol.

glycoside of L-cysteinyl-D-glucosaminyl-L-malate and is a significant LMW thiol found in *S. aureus*. Like mycothiol in mycobacteria and glutathione in Gram-negative bacteria, BSH serves as the LMW thiol responsible for detoxification of xenobiotics in Gram-positive organisms.[21] Recently, the BSH-dependent detoxification of rifamycin in *S. aureus* Newman was shown to result in the mercapturic acid form of the antibiotic, an end compound that is analogous to the products of the mycothiol- and glutathione-dependent detoxification pathways for their respective organisms.[21] Furthermore, BSH knockout strains of both *S. aureus* and *Bacillus subtilis*, along with FosB knockout strains of *B. subtilis*, show increased sensitivity to fosfomycin.[17,22]

In this report, we present five three-dimensional X-ray structures of FosB from *S. aureus* ($FosB^{Sa}$). Two of the structures contain Zn^{2+} and sulfate in the active site of the enzyme: one determined by single-wavelength anomalous dispersion (SAD) phasing to 1.42 Å resolution and the other by molecular replacement to 1.15 Å resolution. In addition to the $FosB^{Sa}$·Zn^{2+}·sulfate structures, we provide structures of $FosB^{Sa}$ cocrystallized with either L-Cys or BSH. Cocrystallization of $FosB^{Sa}$ with the exogenous thiol results in removal of the metal and formation of a disulfide bond to the active site Cys9 of the enzyme. In three of the five structures, an alternate conformation of an important active site loop region of the enzyme that provides insight into the mechanism of the FosB enzymes is observed. In addition, we present kinetic analyses to demonstrate that $FosB^{Sa}$ thiol transferase activity is inhibited by Zn^{2+} at physiological concentrations (~100 μM). Finally, we provide disk diffusion assays to show that *S. aureus* inactivated for FosB in both the Newman and USA300 JE2 strain backgrounds exhibits increased susceptibility to fosfomycin. Thus, this report contains the crystal structure of the fosfomycin resistance enzyme from *S. aureus* and demonstrates that the enzyme is required for resistance of the pathogen to the antibiotic.

MATERIALS AND METHODS

General Materials. Buffer salts were purchased from Research Products International Corp. (RPI) and used without further purification. All crystallization materials were from Hampton Research. Metals were obtained as their chloride salts from J. T. Baker. L-Cysteine was purchased from Sigma Life Sciences. Fosfomycin disodium salt was from MP Biomedicals, LLC. BSH was synthesized as bacillithiol disulfide (BSSB) by the Vanderbilt Chemical Synthesis Core and reduced to BSH prior to use according to published procedures.[19] pET28 ($FosB^{Sa}$) was from Platinum PCR SuperMix, and custom primers were ordered from Invitrogen (Carlsbad, CA). Restriction enzymes were from New England Biolabs (Ipswich, MA). The pET20b(+) vector was from EMB Chemicals, Inc. (Gibbstown, NJ). XL1-Blue supercompetent cells and BL21-Gold (DE3) cells were from Agilent Technologies (Santa Clara, CA).

Protein Expression and Purification for Crystallography and Kinetics. *N-Terminal Intein-Tagged $FosB^{Sa}$.* Intein-tagged $FosB^{Sa}$ was expressed and purified for crystallography as previously described.[19] Intein-tagged $FosB^{Sa}$ was dialyzed into 25 mM HEPES (pH 7.5) containing 50 mM NaCl.

N-Terminal Six-His-Tagged $FosB^{Sa}$. The six-His $FosB^{Sa}$ gene was amplified from the $FosB^{Sa}$-pET28 plasmid previously prepared[19] using primers containing restriction sites for *Nde*I and *Eco*RI. To prepare the N-terminal six-histidine-tagged $FosB^{Sa}$ construct, the forward primer was 5′-GC GGG GCC GGG GGT ATA **CAT ATG** CAT CAT CAT CAT CAT CAC TTA AAA TCT ATT AAT C-3′ and the reverse primer was 5′-GCC GGC GCC CG**G AAT TC**G CTT ATT TGT AAA ATG-3′. The underlined parts of primer sequences are complementary to the nucleotide sequences of the $FosB^{Sa}$-pET28 gene, whereas the 5′-overhanging ends of primers contain recognition sites for restriction endonucleases (bold) and are designed to facilitate cloning.

The polymerase chain reaction (PCR) solution consisted of 200 ng of pET28($FosB^{Sa}$), each primer at 10 μM, and 45 μL of Platinum PCR SuperMix. For PCR, 35 cycles were performed with a temperature profile of 30 s at 95 °C, 30 s at 55 °C, and 1 min at 72 °C in an Applied Biosystems (Foster City, CA) 2720 thermal cycler. The amplification products were analyzed by electrophoresis on a 0.8% agarose gel stained with ethidium bromide.

The amplification products (1 μg) and pET20b vector (1 μg) were digested with *Nde*I and *Eco*RI. The digested DNA was analyzed by electrophoresis as previously described; the corresponding bands on the gel were excised, and the DNA was extracted with a QIAquick Gel Extraction Kit (Qiagen). Purified histidine-tagged $FosB^{Sa}$ and nontagged $FosB^{Sa}$ were each ligated into pET20b *Nde*I−*Eco*RI sites. *Escherichia coli* XL1-Blue supercompetent cells were transformed with the ligation mixture, and four colonies were assayed for the presence of the $FosB^{Sa}$ gene fragment by plasmid extraction and plasmid DNA sequencing.

The new pET-20b expression plasmid containing the gene encoding six-His-tagged $FosB^{Sa}$ was transformed into *E. coli* BL21(DE3) cells. The cells were plated on LB-agar containing 100 μg/mL ampicillin and incubated at 37 °C for approximately 16 h. Single colonies were isolated from the

dx.doi.org/10.1021/bi4015852 | *Biochemistry* 2014, 53, 755−765

Table 1. Data Collection and Refinement Statistics

	FosB·Zn·sulfate SAD	FosB·Zn·sulfate MR	FosB·BS-Cys9	FosB·L-Cys-Cys9	apo FosB
Protein Data Bank entry	4NAY	4NAZ	4NB0	4NB1	4NB2
space group	*C*2	*C*2	*P*1	*P*1	*P*1
unit cell parameters					
a (Å)	62.49	62.62	40.93	40.88	40.61
b (Å)	62.91	62.81	44.88	44.92	44.83
c (Å)	44.91	45.05	46.87	46.35	45.67
α (deg)	90.00	90.00	110.91	61.19	119.30
β (deg)	121.91	122.08	115.24	65.04	106.79
γ (deg)	90.00	90.00	98.27	82.5	97.92
			Data Collection		
temperature (K)	100	100	100	100	100
wavelength (Å)	1.2823	1.0781	1.1272	1.5412	1.5412
resolution (Å)[a]	40.56−1.42 (1.44−1.42)	40.53−1.15 (1.17−1.15)	39.27−1.62 (1.65−1.62)	39.19−1.80 (1.85−1.80)	38.88−1.89 (1.94−1.89)
no. of unique reflections	27859	49038	32205	23472	18192
completeness (%)[a]	99.9 (100)	93.6 (89.2)	96.3 (93.9)	97.4 (80.7)	90.0 (80.3)
R_{merge} (%)[b]	5.2 (40.2)	3.9 (29.9)	3.2 (35.3)	6.0 (22.5)	5.5 (34.3)
I/σ	50.8 (4.1)	37.1 (3.1)	24.1 (2.0)	14.4 (2.7)	25.3 (3.6)
redundancy	7.1 (6.0)	3.8 (3.1)	2.0 (2.0)	3.6 (1.3)	2.5 (1.3)
			Refinement		
R_{work}/R_{free} (%)[c]	12.95/16.64	13.44/16.22	18.87/22.44	19.47/24.35	18.56/24.08
average *B* factor (Å^2)					
all atoms	19.27	16.96	23.78	20.37	22.97
protein	18.26	15.35	23.49	20.46	22.57
water	29.50	28.76	27.60	21.36	28.36
no. of atoms					
protein	1244	1375	2204	2218	2245
water	101	136	119	99	162
root-mean-square deviation from ideal					
bond lengths (Å)	0.025	0.025	0.023	0.019	0.020
bond angles (deg)	2.28	2.28	2.22	1.96	2.03
Ramachandran plot (%)[d]					
most favored	110	110	194	202	195
allowed	7	9	22	15	21
disallowed	0	0	0	0	0

[a]Values in parentheses are for the highest-resolution shell. [b]$R_{merge} = \sum(|I - \bar{I}|)/\sum I \times 100$. [c]$R_{work} = \sum|F_o - F_c|/\sum F_o \times 100$, where F_o is the observed structure factor amplitude and F_c is the calculated structure factor amplitude. [d]Values are numbers of residues.

LB-agar plates and used to inoculate 2 mL LB (Gibco) starter cultures (three cultures for a total of 6 mL) containing 80 μg/mL ampicillin. After incubation at 37 °C for ∼8 h with shaking, 1 mL of starter growth was used to inoculate 1 L of Terrific Broth containing 80 μg/mL ampicillin (6 L total). The 1 L cultures were grown at 37 °C while being shaken for approximately 12 h (or until the OD_{600} reached ∼1) and then induced with 0.5 mM IPTG. Upon induction with IPTG, the temperature was reduced to 25 °C and the cells were allowed to grow for an additional 4−5 h. The cells were harvested by centrifugation at 5000*g* for 15 min.

The *E. coli* cell pellet was resuspended in 2 mL of His tag lysis buffer [50 mM sodium phosphate (pH 8.0), 300 mM sodium chloride, and 10 mM imidazole] per gram of cell pellet. Lysozyme was added to the slurry at a concentration of 1 mg/mL, and the mixture was stirred at 4 °C for 1 h. After the mixture had been stirred for 1 h, 5 mg of DNase and RNase were added, and the slurry was stirred at 4 °C for an additional 1 h. The slurry was sonicated to ensure complete lysing of cells and the lysate cleared by centrifugation at 35000*g* for 30 min.

The cleared lysate containing the six-His-tagged FosB protein of interest was added to a nickel-NTA purification column. The column was washed with 50 mM NaH_2PO_4 (pH 8.0) containing 300 mM NaCl and 20 mM imidazole to remove any protein impurities. Finally, the six-His-tagged FosB protein was eluted form the nickel-NTA column with 50 mM NaH_2PO_4 (pH 8.0), containing 300 mM NaCl and 250 mM imidazole. Following elution from the column, the FosB protein was dialyzed into 20 mM HEPES (pH 7.5) for crystallization trials.

dx.doi.org/10.1021/bi4015852 | *Biochemistry* 2014, 53, 755−765

Protein Crystallization. *N-Terminal Intein-Tagged FosB^{Sa}.* Crystals of intein-tagged FosB^{Sa} with the exogenous L-Cys-Cys9 disulfide bond were grown using the hanging drop vapor diffusion method at 303 K by mixing 3 μL of protein solution [20 mg/mL in 25 mM HEPES buffer (pH 7.5), 50 mM NaCl, 10 mM $MgCl_2$, 10 mM L-Cys, and 10 mM fosfomycin] and 3 μL of reservoir solution [Hampton Research Index 68, 0.1 M HEPES (pH 7.5), 200 mM ammonium sulfate, and 25% (w/v) polyethylene glycol (PEG) 3350] in a Hampton Research VDX plate. Apo crystals of intein-tagged FosB^{Sa} were grown via the same approach with the addition of 10 mM tris(2-carboxyethyl)phosphine (TCEP) to the initial protein solution. These crystals were cryoprotected with 25% ethylene glycol in 75% mother liquor.

N-Terminal Six-His-Tagged FosB^{Sa}. Initial crystals of six-His-tagged FosB^{Sa} (Figure S1 of the Supporting Information) were grown using the hanging drop vapor diffusion method at 303 K by mixing 3 μL of protein solution [8 mg/mL in 20 mM HEPES buffer (pH 7.5)] and 3 μL of reservoir solution [Hampton Research Index 67, 0.1 M Bis-Tris (pH 6.5), 200 mM ammonium sulfate, and 25% (w/v) PEG 3350] in a Hampton Research VDX plate. The final optimized conditions for each crystal are as follows. The FosB^{Sa} crystals with Zn^{2+} and sulfate used for SAD phasing and molecular replacement were obtained after mixing equal volumes (3 μL) of protein solution [7.5 mg/mL in 20 mM HEPES buffer (pH 7.5) and 5 mM fosfomycin] and reservoir solution [0.1 M Bis-Tris (pH 6.5), 200 mM ammonium sulfate, and 16% (w/v) PEG 3350]. The FosB^{Sa} crystals with bacillithiol were obtained after mixing equal volumes (3 μL) of protein solution [7.5 mg/mL in 20 mM HEPES buffer (pH 7.5), 5 mM fosfomycin, and 5 mM BSH] and reservoir solution [0.1 M Bis-Tris, 200 mM ammonium sulfate, and 16% (w/v) PEG 3350]. All crystals were cryoprotected in 30% glycerol and 70% mother liquor and frozen in liquid nitrogen prior to collection of the diffraction data.

Data Collection and Refinement. Diffraction data for all crystals were collected at 100 K on either the LS-CAT 21-ID beamline at the APS synchrotron facility or the Bruker-Nonius Microstar rotating anode X-ray generator at Vanderbilt University. The collected diffraction data sets from LS-CAT 21-ID were processed with HKL2000,[23] whereas those collected on the Bruker instrument were processed with Bruker-AXS (2010) PROTEUM2 version 2010.11 (Bruker-AXS, Madison, WI). Phasing of the diffraction data was done either by SAD phasing using SHELXD/E[24] or by molecular replacement using PHASER.[25] For SAD phasing, the presence of anomalous scatterers was confirmed and the peak wavelength was determined by X-ray fluorescence. In the case of SAD phasing, the initial model was constructed using ARPwARP.[26] For molecular replacement, the first model output and refined from ARPwARP was used as the initial search model. Manual model building for each structure was performed using Coot model building software.[27] Waters were placed with the Coot routine, Find Waters. The final models were obtained by iterative cycles of model building in Coot and structure refinement using Refmac5[28] in the CCP4 suite of programs (Collaborative Computational Project, 1994). All protein figures were prepared with Chimera.[29] Data collection and refinement statistics are listed in Table 1.

Continuous ^{31}P NMR Activity Assays with Zn^{2+}. FosB^{Sa} (0.5 μM) was equilibrated for 5 min with 100 μM $ZnCl_2$ and 8 mM fosfomycin in 20 mM HEPES (pH 7.0). The reaction was initiated by addition of 1.8 mM BSH or L-Cys, and the mixture was transferred to an NMR tube and allowed to react at room temperature. At various time points, a ^{31}P with ^{1}H decoupling NMR spectrum was collected using Bruker AV-400 MHz NMR. The analysis of the data was completed according to the method previously described.[19]

Time Point High-Performance Liquid Chromatography (HPLC) Activity Assays with Mn^{2+} and Mn^{2+} with Zn^{2+}. FosB^{Sa} (0.5 μM) was equilibrated for 5 min with either 10 μM $MnCl_2$ or 10 μM $MnCl_2$ and 100 μM $ZnCl_2$ and 4 mM fosfomycin in 20 mM HEPES (pH 7.0). The reaction was initiated by addition of 1.6 mM BSH or 1.8 mM L-Cys and the mixture allowed to react at room temperature. At various time points, a 20 μL aliquot of the reaction mixture was quenched by addition of 40 μL of 5% (w/v) trichloroacetic acid followed by vortexing. Addition of 15 μL of 0.8 M NaOH returned the pH to 7.0. An internal standard (20 μL of 0.4 mM serine) was added, and the mixture was diluted to 100 μL with 20 mM HEPES (pH 7.0). A 20 μL aliquot of the quench was added to 55 μL of borate buffer and mixed with 25 μL of the AQC reagent (Waters, Milford, MA) solubilized according to the manufacturer's directions. Derivatization reaction mixtures were incubated at 55 °C for 10 min followed by dilution with 400 μL of 70 mM NaOAc containing 7 mM triethylamine, adjusted to pH 5.0 with phosphoric acid (mobile phase A).

Derivatized samples were analyzed on an Agilent 1260 Infinity HPLC System using fluorescence detection with excitation at 250 nm and emission at 395 nm. Samples were injected onto a 250 mm × 4.6 mm Kinetex C-18 column with a particle size of 5 μm and a pore size of 100 Å (Phenomenex, Torrance, CA) and equilibrated with 90% mobile phase A and 10% mobile phase B [80% (v/v) acetonitrile]. Samples were eluted using a flow rate of 1 mL/min and the following gradient of mobile phase B: 10% from 0 to 6 min, 10 to 12% from 6 to 12 min, 12 to 15% from 12 to 15 min, 15 to 40% from 15 to 19 min, and 40 to 100% from 19 to 22 min. BS-fosfomycin, L-Cys-fosfomycin, and serine had retention times of 4.0, 4.7, and 7.5 min, respectively. The amount of product formed was quantified as previously described.[30]

Disk Diffusion Assay. Soft agar was inoculated with an overnight culture of Newman or USA300 JE2 methicillin-resistant *S. aureus* isolate and poured over a tryptic soy agar plate. Four sterile Whatman paper discs were placed on top of the cooled soft agar. The indicated amounts of fosfomycin were added to each disk from a 50 mg/mL stock. The plates were incubated overnight at 37 °C.

RESULTS

Crystal Structure Determination and Modeling. *FosB^{Sa} with Zinc and Sulfate, SAD Phasing [Protein Data Bank (PDB) entry 4NAY].* The crystal structure of the FosB^{Sa}·Zn^{2+}·sulfate complex was refined to 1.42 Å resolution (Figure 3). An X-ray fluorescence scan of the crystal prior to collection of the diffraction data indicated the presence of Zn^{2+} (Figure S2 of the Supporting Information). Subsequently, the diffraction data were collected at a wavelength of 1.28 Å, the K_α absorption edge of Zn^{2+}, and the initial phases were determined using Zn^{2+} SAD phasing. This crystal indexed into the *C*2 space group. Unit cell content analysis of the data indicated one subunit of FosB^{Sa} and one metal ion per asymmetric unit. The anomalous density map, contoured at 5σ, is displayed in Figure 3 and outlines the location of the Zn^{2+} metal ions used in the model.

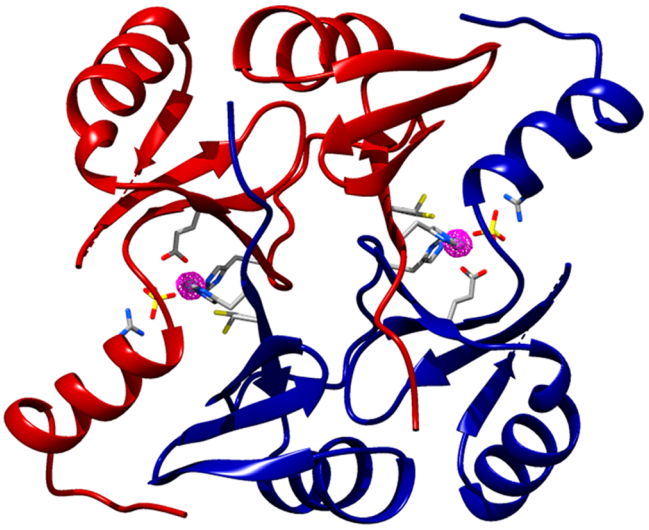

Figure 3. Overall crystal structure of FosB from *S. aureus* with Zn^{2+} and sulfate in the active site. The structure was determined by SAD phasing from the Zn^{2+} K_α edge. The red and blue color scheme indicates each subunit of the homodimer of the enzyme after the symmetry operation has been applied to the coordinate file. The anomalous density map (magenta) around the Zn^{2+} metal ions (purple) is contoured at 5σ and clearly marks the location of the metal within the structure. Final refinement yielded an R_{work} of 12.95% and an R_{free} of 16.64%.

The final model consists of amino acids 1−91 and 102−138 with a sulfate ion coordinated to the metal.

FosB^{Sa} with Zinc and Sulfate, Molecular Replacement (PDB entry 4NAZ). After the initial crystal structure of the FosB^{Sa}·Zn^{2+}·sulfate had been determined by SAD phasing, another data set was collected on a second crystal at a wavelength of 1.078 Å to achieve higher resolution. The second data set, determined by molecular replacement using PDB entry 4NAY, resulted in a 1.15 Å resolution structure of FosB^{Sa} with Zn^{2+} and sulfate in the active site (Figure S3 of the Supporting Information). Zn^{2+} was used to model the metal ion density in the active site given that the enzyme was expressed, purified, and crystallized under the same conditions as PDB entry 4NAY. This crystal also indexed into the *C*2 space group with one subunit of FosB^{Sa} per asymmetric unit. The final model consists of amino acids 1−91 and 102−139 with a sulfate ion coordinated to the metal.

FosB^{Sa} with a Bacillithiol−Cys9 Disulfide Bond (PDB entry 4NB0). Cocrystallization of FosB^{Sa} with BSH resulted in a crystal structure of the enzyme with a BS-Cys9 disulfide bond (Figures S4 and S5 of the Supporting Information). X-ray fluorescence scans of the crystal prior to collection of the diffraction data did not indicate the presence of any metals (Figures S6 and S7 of the Supporting Information). This crystal indexed into the *P*1 space group, rather than *C*2, and had both subunits of the homodimer in the asymmetric unit. The structure was determined by molecular replacement using a homodimer model of the enzyme created from PDB entry 4NAZ. The final resolution of this structure is 1.62 Å, and the final model consists of amino acids 1−53, 62−91, 102−128, and 133−138 for subunit A and 1−53, 63−129, and 135−138 for subunit B.

FosB^{Sa} with an L-Cysteine−Cys9 Disulfide Bond (PDB entry 4NB1). Cocrystallization of FosB^{Sa} with L-Cys resulted in a crystal structure with an L-Cys−Cys9 disulfide bond similar to that with BSH (Figures S8 and S9 of the Supporting Information). This crystal also indexed into the *P*1 space group, was determined by molecular replacement, and had a final resolution of 1.62 Å. The final model consists of amino acids 1−52, 61−92, 102−127, and 131−139 for subunit A and 1−53, 64−128, and 134−138 for subunit B.

FosB^{Sa} Apo Structure (PDB entry 4NB2). Cocrystallization of FosB^{Sa} with L-Cys and TCEP reduced the exogenous disulfide bond and yielded an apo structure of the enzyme (Figure S10 of the Supporting Information). The resultant structure indexed into the *P*1 space group and had a final resolution of 1.62 Å. The final model consists of amino acids 1−56, 62−91, 102−126, and 132−138 for subunit A and 1−53, 63−128, and 135−138 for subunit B.

Overall Structure of FosB^{Sa}. Similar to the FosB enzymes from *Bacillus cereus*[31] and *Bacillus anthracis*, FosB^{Bc} and FosB^{Ba}, respectively, FosB^{Sa} belongs to the vicinal oxygen chelate (VOC) superfamily of enzymes. Although amino acids 92−101 are not observed in PDB entry 4NAY or 4NAZ and are observed in only one subunit of PDB entries 4NB0, 4NB1, and 4NB2, the three-dimensional domain-swapped arrangement of sequential $\beta\alpha\beta\beta\beta$ motifs that define the VOC superfamily is still evident in the overall structure (Figure 3 and Figures S3, S4, S8, and S10 of the Supporting Information).[32] The protein residues that constitute the metal binding site in FosB^{Sa} are His7, His66, and Glu115, the same as those in FosB^{Bc}.[31] In the FosB^{Sa}·Zn^{2+}·sulfate structures (PDB entries 4NAY and 4NAZ), the Zn^{2+} adopts a tetrahedral coordination geometry with a sulfate oxygen occupying the fourth coordination site of the metal. However, the sulfate molecule, in either structure, is oriented in a position opposite to that observed in FosB^{Bc},[31] with the second of the sulfate oxygens hydrogen bonded to the non-metal-coordinated O_ε atom of Glu115 (Figure 4, left). In

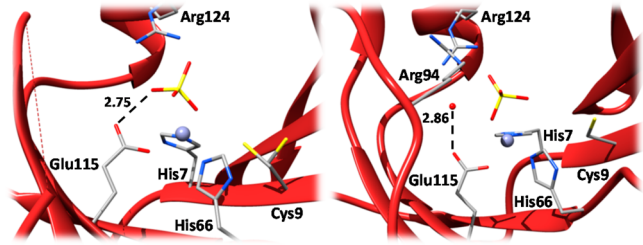

Figure 4. Sulfate molecule of FosB^{Sa} (left) oriented in a position opposite that observed in FosB^{Bc} (right).[31] In FosB^{Sa}, the second of the sulfate oxygens is hydrogen bonded to the non-metal-coordinated O_ε atom of Glu115. In FosB^{Bc}, the non-metal-coordinated O_ε atom of Glu115 is hydrogen bonded to a highly conserved water molecule. Cys9 in the FosB^{Sa} structure is observed in two conformations, pointed toward or away from the metal. The occupancy of the two conformations is correlated to the occupancy of Zn^{2+} and the coordinated sulfate molecule such that the occupancy of Cys9 pointed away from the metal is approximately the same as that for the metal and the coordinated sulfate molecule.

FosB^{Bc} (PDB entry 4JH2), the sulfate is oriented in a position that superimposes the phosphonate moiety of fosfomycin, and the non-metal-coordinated O_ε atom of Glu115 is hydrogen bonded to a highly conserved water molecule (Figure 4, right).

Alternate Conformation of the Fosfomycin−Phosphonate Binding Loop. In PDB entries 4NB0 (FosB^{Sa} with a BS−Cys9 disulfide bond), 4NB1 (FosB^{Sa} with an L-Cys−Cys9 disulfide bond), and 4NB2 (FosB^{Sa} apo structure), amino acids ~90−101 are observed in a conformation different from that

dx.doi.org/10.1021/bi4015852 | *Biochemistry* 2014, 53, 755−765

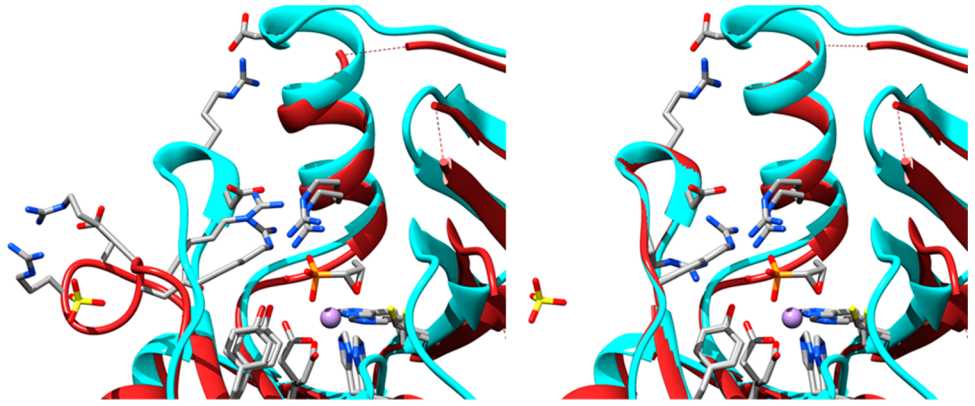

Figure 5. Superposition of FosB^{Bc} (cyan) and FosB^{Sa} (red) (left). In the FosB^{Bc} structure (PDB entry 4JH6), Mn^{2+} and fosfomycin are bound in the active site and the conserved phosphonate binding loop is observed in the closed conformation. In the FosB^{Sa} structure (PDB entry 4NB2), there is no metal or antibiotic bound in the active site. Therefore, the phosphonate binding loop is observed in the open conformation. Superpostion of FosB^{Bc} and FosB^{Sa} with the phosphonate binding loop morphed into the closed conformation (right). The conserved fosfomycin cage residues align after the FosB^{Sa} structure has been morphed into the FosB^{Bc} structure.

found in either FosB^{Bc} or FosB^{Ba} (Figure 5, left). The two different conformations can be described as open, for FosB^{Sa}, and closed, for both FosB^{Bc} and FosB^{Ba} (PDB entry 4IR0, not shown), the difference being the absence and presence of fosfomycin, respectively. In the structures of FosB^{Sa} with the open loop conformation, the loop region is wrapped around a sulfate molecule (Figure 5 and Figures S4, S8, and S10 of the Supporting Information). Of the approximately 11 residues that compose the loop region, eight are conserved throughout all the FosB enzymes (Figure 6). The three nonconserved residues

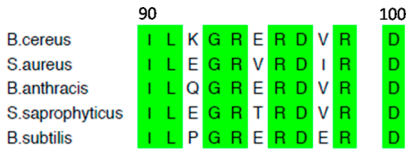

Figure 6. Sequence alignment of the phosphonate binding loop residues. Eight of the 11 residues are conserved throughout the FosB enzymes. The nonconserved residues are all solvent-exposed.

are solvent-exposed in the closed conformation of the loop in the FosB^{Bc} (PDB entry 4JH6) or FosB^{Ba} (PDB entry 4IR0) structure. The conserved residues of the loop region constitute important structural features of the enzyme. In the closed conformation, they form one side of the fosfomycin binding cage with several hydrogen bonding interactions to the antibiotic and also form one side of the BSH binding pocket. Most importantly, the open residues of FosB^{Sa} can be morphed into the positions of fosfomycin-bound FosB^{Bc} to completely form the important substrate binding structural features (Figure 5, right).

Kinetic Analysis. A detailed mechanistic investigation of divalent metal activation of FosB^{Sa} has been reported.[33] The results indicated that FosB^{Sa} is activated by Zn^{2+} and has the following metal ion activation order: Zn^{2+} > Ni^{2+} > Mn^{2+} > Mg^{2+} ~ Fe^{2+} ~ Co^{2+} ~ Cu^{2+} ~ Ca^{2+}. However, this result is contradictory to the metal activation of all other fosfomycin resistance enzymes from the VOC superfamily, including FosA, FosX, FosB^{Bc}, and FosB^{Bs}, in which Zn^{2+} effectively inhibits any transferase activity.[7,8,12,18,19,31] Therefore, when we obtained the crystal structure of FosB^{Sa} with Zn^{2+} in the active site, we were compelled to confirm the reported results.[33]

Our time course kinetic analyses, shown in Figure 7, indicate that FosB^{Sa} is inhibited for L-Cys transferase activity and only

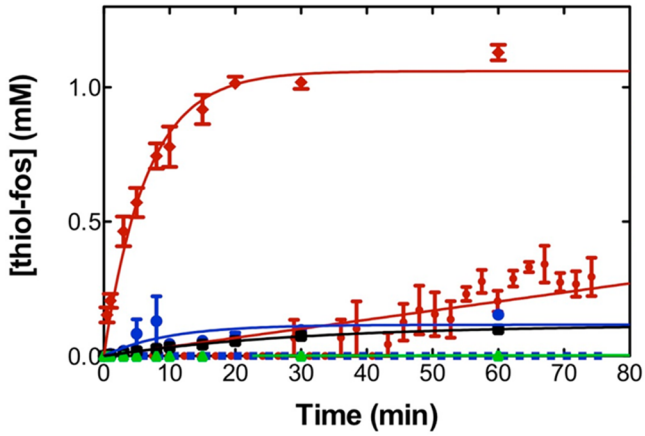

Figure 7. Time course of FosB^{Sa}-catalyzed addition of BSH or L-Cys to fosfomycin in the presence of Mn^{2+} or Zn^{2+}. Reactions were conducted at 25 °C in 20 mM HEPES (pH 7.0) with 4 mM fosfomycin and 0.50 μM enzyme in the presence of (red diamonds) 1.6 mM BSH and 10 μM Mn^{2+}, (red circles) 1.6 mM BSH and 10 μM Zn^{2+}, (blue circles) 1.6 mM BSH, 10 μM Mn^{2+}, and 100 μM Zn^{2+}, (black squares) 1.8 mM L-Cys and 10 μM Mn^{2+}, (blue squares) 1.8 mM L-Cys and 10 μM Zn^{2+}, or (green triangles) 1.8 mM L-Cys, 10 μM Mn^{2+}, and 100 μM Zn^{2+}.

marginally active for BSH transferase activity at physiological concentrations of Zn^{2+} (~100 μM)[34] with an apparent k_{cat}^{BSH} of 0.17 s^{-1}. In addition, we found that 10 μM Mn^{2+} activates FosB^{Sa} for BSH transferase activity with an apparent k_{cat}^{BSH} of 5.98 s^{-1}. These results are consistent with other reports for VOC class fosfomycin resistance enzymes.[7,8,12,18,19,31] By comparison, the apparent k_{cat} for L-Cys transferase activity of FosB^{Sa} activated by physiological concentrations of Mn^{2+} (~10 μM)[34] is 0.05 s^{-1}, indicating that FosB^{Sa} has a preference for BSH in agreement with published results.[19,33] Finally, we found that 100 μM Zn^{2+} inhibits the reaction when the mixture is supplemented with 10 μM Mn^{2+} for either L-Cys or BSH transferase activity. The apparent k_{cat}^{BSH} is 0.08 s^{-1}, whereas the apparent $k_{cat}^{L\text{-}Cys}$ could not be determined, similar to inhibition by Zn^{2+} alone.

dx.doi.org/10.1021/bi4015852 | *Biochemistry* 2014, 53, 755−765

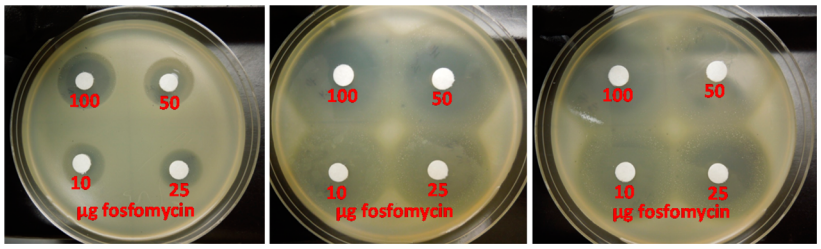

Figure 8. Fosfomycin disk diffusion assays for USA300 JE2 (MRSA). The amount of fosfomycin on each disk is shown in red: (left) wild-type MRSA, (center) BshA knockout MRSA, and (right) FosB knockout MRSA.

Disk Diffusion Assays. Our kinetic analysis, in addition to the previous kinetic analyses,[19,31] has demonstrated that FosB enzymes have a preference for BSH over L-Cys for nucleophilic addition to fosfomycin *in vitro*. Furthermore, the pathway for detoxification of xenobiotics (including fosfomycin) involving BSH has been characterized for *S. aureus in vivo*.[21] While BSH null *S. aureus* exhibited an increase in sensitivity to fosfomycin for both the Newman[17] and USA300 JE2 strains, the question of whether FosB null *S. aureus* exhibits a similar increase in sensitivity to the antibiotic remained. To answer this, *bshA*, which encodes the glycosyltransferase involved in BSH biosynthesis, and *fosB* knockout strains of both Newman and USA300 JE2 *S. aureus* were obtained from the Network on Antimicrobial Resistance in *S. aureus* (NARSA), and Kirby-Bauer disk diffusion assays were conducted on the prepared cultures to test their sensitivity to fosfomycin. As anticipated, both the BSH and FosB null strains of USA300 JE2 and Newman show a substantial increase in their sensitivity to the antibiotic as evidenced by the increased zone of clearing (Figure 8 and Figure S11 of the Supporting Information, summarized in Table 2). Furthermore, the zone of clearing of the BshA null mutant is comparable to that of the FosB null mutant, indicating that both BSH and the FosB enzyme are required for optimal survival of *S. aureus* when it is treated with fosfomycin.

Table 2. Disk Diffusion Zones of Clearing (millimeters) for MRSA

strain	10 μg	25 μg	50 μg	100 μg
WT USA300 JE2	17	18	21	24
BshA KO	34	33	40	40
Fosb KO	35	33	37	40
WT Newman	22	24	28	30
BshA KO	35	37	40	40
Fosb KO	34	34	39	37

DISCUSSION

Structural Interpretation of FosB^{Sa}. The 139-amino acid FosB enzyme reported here is conserved throughout the *S. aureus* genome sequences available in UniProt, including the USA300 JE2 (MRSA) and Newman (NCTC 8325) strains. Thus, the reported three-dimensional structures are representative of the same resistance enzyme from both strains of the pathogen.

FosB^{Sa} crystallized with Zn^{2+} in the active site of the enzyme, as did FosB from *B. cereus* (FosB^{Bc}).[31] The Zn^{2+} in the active site is most likely a result of the nutrient rich Terrific Broth used during protein expression. Having Zn^{2+} in the active site is fortuitous because, of the first-row transition metals found in most biological macromolecules, Zn^{2+} has the greatest electron density and is therefore one of the best anomalous scatterers. Thus, Zn^{2+} gives a very strong X-ray fluorescence signal (Figure S2 of the Supporting Information) and is an excellent metal for SAD phasing of the data. The anomalous scattering density map shown in Figure 3 establishes the location of the metal ion in the active site of the enzyme. However, at a given wavelength, several metals will give an anomalous signal, and the correct metal need not be assigned to determine the structure by SAD methods. Thus, we have used Zn^{2+} to model the anomalous electron density, but we recognize that the metal may not be homogeneously distributed throughout the entire crystal.

Although both FosB^{Bc} and FosB^{Ba} were crystallized with fosfomycin coordinated to the metal, we have been unable to obtain a fosfomycin-coordinated structure of FosB^{Sa} even though the antibiotic was present in the crystallization solution at a concentration of 5 mM. This is due to the crystallization conditions requiring high concentrations of ammonium sulfate (200 mM) that compete with fosfomycin for binding in the active site of the enzyme. Sulfate molecules have been observed in the active sites of other VOC class fosfomycin resistance enzymes,[12,15,31] as the sulfate ion is isoelectronic with the phosphonate moiety of the antibiotic.

Neither the metal nor the sulfate in PDB entries 4NAY and 4NAZ has an occupancy of 100% in the structures. Rather, Cys9 in the FosB^{Sa} structure is observed in two conformations (Figure 4, left). They can be described as pointing toward or away from the metal ion binding site of the enzyme. The occupancy of the two conformations (~50/50) is correlated to the occupancy of Zn^{2+} and the coordinated sulfate molecule such that the occupancy of Cys9 pointed away from the metal is approximately the same as that for the metal and the coordinated sulfate molecule. The conformation pointed away from the metal binding site is the same as that observed for FosB from *B. cereus*[31] and FosB from *B. anthracis* (PDB entry 4IR0). The functional significance of these two conformations is currently not known and may simply be a steric consequence resulting from the metal vacancy.

The most important feature of the structures reported here is the loop region composed of amino acids 90−100. In the structures of FosB^{Bc} and FosB^{Ba}, the loop region is observed in a conformation that encloses the hydrophilic phosphonate end of the polar antibiotic and represents one side of the "fosfomycin cage" structure of the enzyme.[31] The fosfomycin cage is composed of residues Tyr39, Trp46, Ala48, Tyr64, Arg94, Asp100, Tyr105, and Arg124, all of which are conserved (FosB^{Bc} of Figure 5, or see Figure 9 of ref 31 for greater detail), and is the structural feature that locks the antibiotic in the active site properly positioning C1 for nucleophilic attack by L-Cys or BSH. In FosB^{Sa}, the residues are highly dynamic as

dx.doi.org/10.1021/bi4015852 | *Biochemistry* 2014, 53, 755−765

evidenced by the complete lack of electron density for the region in either PDB entry 4NAY or 4NAZ, suggesting a high degree of flexibility. In PDB entries 4NB0, 4NB1, and 4NB2, electron density for the residues is observed, but the loop is in a conformation that can be described as "open" relative to FosB^{Bc} or FosB^{Ba} (Figure 5 and Figures S4, S8, S10, and S12 of the Supporting Information).

In both the FosB^{Bc} and FosB^{Ba} structures, the phosphonate moiety of fosfomycin is directly coordinated by Arg94 of the loop and/or cage, which also forms a salt bridge with Asp100 giving rigidity to the cage (see Figure 9 of ref 31). Arg96 is hydrogen bonded to Tyr105 and to a highly conserved water molecule that is hydrogen bonded to the non-metal-coordinated O_ε atom of Glu115. The water molecule coordinated to the O_ε atom of Glu115 is also hydrogen bonded to one phosphonate oxygen and Arg124 of the cage. It has been observed in every deposited structure of FosB to date (Figure 4, Right). However, its position is approximately 5 Å from C1 of the antibiotic in FosB^{Bc}, and given that nucleophilic addition of the thiol proceeds via direct S_N2 substitution to C1, the functional relevance of the conserved water in the active site of FosB has remained unclear. In PDB entries 4NAY and 4NAZ, both the water and fosfomycin are absent, and the sulfate is positioned "backward" relative to FosB^{Bc} (PDB entry 4JH2), with one oxygen coordinated to the metal and another coordinated to the second O_ε atom of Glu155, where the conserved water molecule is expected (Figure 4, left). As a result, the residues of the loop region have nothing to coordinate and are highly dynamic, leading to inhomogeneity in the crystal and no observed electron density.

In PDB entries 4NB0, 4NB1, and 4NB2, where the open conformation of the loop is observed, the residues of the loop are wrapped around a sulfate molecule forming five hydrogen bond interactions and demonstrating the propensity of the loop to coordinate sulfate or perhaps the isoelectronic phosphonate end of fosfomycin (Figure 5 and Figures S4, S8, S10, and S12 of the Supporting Information). The open conformation of the phosphonate binding loop in the structures of FosB^{Sa} presented here points to an important functional aspect of the enzyme. In both the FosB^{Bc} and FosB^{Ba} structures, only a narrow access channel leading to C1 of the antibiotic is observed. In FosB^{Bc}, the cross-sectional area of the access channel at its most narrow point is approximately 15 Å^2 (Figure S13 of the Supporting Information), whereas the cross-sectional area of the phosphonate end of fosfomycin is 19 Å^2 (Figure S14 of the Supporting Information). Moreover, the narrow channel is optimized to accommodate the L-cysteinyl domain of BSH and contains conserved residues involved in the catalytic mechanism of the FosB enzymes. This raises the question of how fosfomycin enters the interior active site of FosB.

We think the answer lies in opening and closing of the loop region. The loop must be open to allow fosfomycin to enter the interior cavity of FosB. The hydrophobic methyl end of the antibiotic would thermodynamically favor the hydrophobic side of the fosfomycin cage of the enzyme. Once bound, the loop closes around the antibiotic holding it in place directly at the end of the access channel poised for nucleophilic attack by the thiol. Loop closure could incorporate the unexplained water molecule, and a combination of hydrogen bonds to the water and to the antibiotic would hold the loop in its closed position forming the final side of the BSH binding pocket (see Figure 7 of ref 31). This ordered substrate binding mechanism involving the loop is consistent with substrate binding studies of FosB^{Sa} that have indicated the antibiotic must bind first followed by nucleophilic attack of the thiol cosubstrate.[33]

When FosB^{Sa} was cocrystallized with either BSH or L-Cys, a disulfide bond formed between the exogenous thiol and Cys9 of the enzyme (Figures S5 and S9 of the Supporting Information). When the disulfide bond is present in the structure, the metal is removed from the active site of the enzyme. The conformation of Cys9 in the disulfide bond is that pointed away from the metal binding site, as in FosB^{Bc} and FosB^{Ba}. The crystals containing the unnatural disulfide bonds belong to a space group ($P1$) different from that of those that contain Zn^{2+} and sulfate ($C2$). In PDB entry 4NB1, the density for exogenous L-Cys is very clear. However, in PDB entry 4NB0, the density for BSH is not complete (Figure S5 of the Supporting Information). This has been observed before in a structure of FosB^{Bc} (PDB entry 4JH9) in which the highly flexible glucosamine−malate moiety of the BSH molecule is not homogeneous in the crystal. The same situation has most likely occurred in the current structure. Nevertheless, given that the crystallization conditions are the same for PDB entry 4NAZ ($C2$) and PDB entry 4NB0 ($P1$) except for addition of BSH, this suggests that a significant change occurred in the enzyme prior to crystallization, indicating that the dilsulfide bond likely formed in solution before the crystals grew, i.e., opening of the phosphonate binding loop. The disulfide bond between L-Cys or BSH and Cys9 is unique to FosB^{Sa} and was never observed in FosB^{Bc} even though the crystallization conditions for FosB^{Bc} included the same concentration of either thiol.[31]

Cocrystallization of FosB^{Sa} with tris(2-carboxyethyl)-phosphine (TCEP) and L-Cys prevented formation of the disulfide bond in the crystal. This resulted in an apo structure of the enzyme with no metals or exogenous ligands in the active site [PDB entry 4NB2 (Figure S5 of the Supporting Information)]. This crystal indexed also into the $P1$ space group even though the disulfide bond was not present. The significance of this structure is that it maintains the open loop conformation even in the absence of any exogenous ligands in the active site of FosB^{Sa}. Thus, the $P1$ space group appears to be the result of the open conformation of the phosphonate binding loop.

Kinetic Analysis of FosB^{Sa}. Initial kinetic analyses of FosB^{Sa} indicated that the enzyme is activated by Zn^{2+} and has the following divalent metal ion activation order: $Zn^{2+} > Ni^{2+} > Mn^{2+} > Mg^{2+} \sim Fe^{2+} \sim Co^{2+} \sim Cu^{2+} \sim Ca^{2+}$.[33] However, other fosfomycin resistance enzymes of the VOC superfamily, including FosA, FosX, FosB^{Bc}, and FosB^{Bs}, are effectively inhibited by Zn^{2+}.[7,8,12,18,19,31] Thus, finding Zn^{2+} in the active site of the FosB^{Sa} structure prompted us to reassess the divalent metal activation and/or inactivation of the enzyme. Our kinetic analysis in Figure 7 was never intended to be a full kinetic report for FosB^{Sa} as we meant to test and confirm the activation of FosB^{Sa} by Zn^{2+}. Nonetheless, as might have been expected given the activation of other VOC class fosfomycin resistance enzymes, we found that FosB^{Sa} is inhibited by Zn^{2+} for L-Cys transferase activity and only marginally active for BSH transferase activity at physiological concentrations (~100 μM).[34] The apparent k_{cat}^{BSH} is only 0.17 s^{-1}. By comparison, the apparent k_{cat}^{BSH} of FosB^{Sa} when it is activated by physiological concentrations of Mn^{2+} (~10 μM) is 5.98 s^{-1}, a >35-fold increase. More interestingly, our kinetic assays involving physiological concentrations of both Zn^{2+} and Mn^{2+} demonstrate that FosB^{Sa} is inhibited for either L-Cys or BSH transferase activity, similar to inhibition by Zn^{2+} alone.

Our kinetic results are in contrast to the published results for $FosB^{Sa}$ specifically[33] but consistent with all other reports for this class of enzymes in which they are activated by Mn^{2+} and inhibited by Zn^{2+}.[7,8,12,18,19,31] Given that active site residues for each class are conserved, especially among the FosB enzymes, we believe that inhibition of $FosB^{Sa}$ by physiological concentrations of Zn^{2+} is correct. It is noteworthy to point out that the published report used concentrations of Zn^{2+} as high as 10 mM in their activation studies, which is physiologically irrelevant. Moreover, an explanation for why this class of enzymes is inhibited by Zn^{2+} and activated by Mn^{2+} has been presented.[31]

Roberts et al. demonstrated that increasing concentrations of BSH (0.5−5 mM) appeared to inhibit activation of $FosB^{Sa}$ by Zn^{2+}, at least until the concentration of Zn^{2+} had eclipsed that of BSH.[33] They concluded that the enzyme and BSH were competing for complexation with Zn^{2+} and that BSH is therefore a sufficiently strong Zn^{2+} chelator to demetalate the enzyme. While BSH is likely an effective M^{2+} chelator by the nature of its functional substituents, our crystals of $FosB^{Sa}$ with disulfide bonds in the active site suggest an alternative explanation. The crystallization conditions presented here [100 mM Bis-Tris (pH 6.5), 5 mM fosfomycin, and 5 mM BSH or 100 mM HEPES (pH 7.5), 10 mM fosfomycin, and 10 mM L-Cys] are similar to the kinetic assay conditions used by Roberts et al. [50 mM HEPES (pH 7.0), 25 mM fosfomycin, and 0.5−5 mM BSH]. Furthermore, the change in crystallographic space group, from *C*2 to *P*1, indicates that the disulfide bond formed in solution prior to crystal formation. Thus, inhibition of $FosB^{Sa}$ by millimolar concentrations of exogenous thiol may be due to formation of the thiol−Cys9 dilsulfide bond and steric removal of the metal rather than demetaltion of the enzyme by the substrate. As a final point, if the BSH were in a strong complex with Zn^{2+}, the thiol would be one of the coordinating ligands, and it would not be able to serve as a nucleophilic substrate for $FosB^{Sa}$. This line of thinking is what prompted our kinetic experiment with both Zn^{2+} and Mn^{2+}. Even if all the Zn^{2+} (100 μM) is in complex with BSH, there is still excess free BSH (1.8 mM) in solution to serve as the nucleophilic substrate for $FosB^{Sa}$ activated by Mn^{2+} (10 μM). Because the reaction does not proceed, we can conclude that either (1) Zn^{2+} and Mn^{2+} are in complex with BSH and there is no free metal to activate the enzyme or (2) Zn^{2+} is competing with Mn^{2+} in the active site of $FosB^{Sa}$ and inhibiting the enzyme. Only the latter conclusion is plausible given that the reaction proceeds as it should in the presense of Mn^{2+} and BSH only.

The interplay between Mn^{2+} and Zn^{2+} for the activation and/or inactivation of $FosB^{Sa}$ is interesting given the importance of acquisition of these two metals for survival of the organism and the concurrent resistance to fosfomycin. The concentrations of Mn^{2+} and Zn^{2+} are very tightly regulated within pathogens like *S. aureus*. Mn^{2+}-dependent superoxide dismutase is encoded by many pathogens to defend against superoxide,[35,36] while an estimated 4−8% of all proteins encoded in the genome of bacteria are Zn^{2+}-binding proteins.[37] Host limitation of nutrient divalent metals is an essential component of the inate immune response to infection by *S. aureus* and other pathogens. In the process of nutritional immunity, neutrophils respond to the infection and deplete the pathogen of vital metals required for proliferation. Specifically, calprotectin binds both Mn^{2+} and Zn^{2+} in an effort to starve the pathogen of the nutrient metals. It is estimated that 40−50% of the protein composition of neutrophil cytoplasm is calprotectin.[38−40] To combat the nutritional immunity of the host, *S. aureus* has evolved high-affinty Mn^{2+} and Zn^{2+} transporters to sequester the required metals necessary for proliferation.[41,42]

Function of $FosB^{Sa}$ *in Vivo*. Regardless of the metal activation and/or inactivation of $FosB^{Sa}$, we were interested in the requirement of the enzyme for survival of the pathogen in general. BSH null strains of *B. subtilis* and *S. aureus* have been examined for their sensitivity to fosfomycin.[17,22] The results consistently demonstrate that BSH is necessary for detoxification of xenobiotics from Gram-positive organisms and that BSH is required for resistance of the organisms to fosfomycin. The disk diffusion assays presented here show that FosB knockout *S. aureus* USA300 JE2 (Figure 8) and Newman (Figure S11 of the Supporting Information) strains demonstrate an increase in susceptibility to fosfomycin similar to that of the BSH null cells. While BshA knockout strains have been examined in the aforementioned BSH null studies, we included them in our experiment for direct comparison to the FosB knockouts. BshA, along with BshB and BshC, is involved in BSH biosynthesis. The zone of clearing for BshA knockout USA300 JE2 cells treated with 100 μg of fosfomycin in our experiment is 40 mm. This result is consistent with the published values of 39, 40, and 39 mm for BshA, BshB, and BshC knockouts, respectively, of USA300 JE2 treated with 350 μg of fosfomycin.[22] While the published data use an amount of fosfomycin more than 3-fold greater than ours, we point out that our results reach a maximal zone of clearing between 25 and 50 μg, and the zone of clearing at 50 μg is the same as that for 100 or 350 μg. Thus, there appears to be a maximal effectiveness of fosfomycin reached for disk diffusion assays somewhere between 25 and 50 μg of the antibiotic. Nevertheless, the zones of clearing for the FosB knockout strains are the same as those for the BshA knockouts, indicating that both the FosB enzyme and BSH are equally important for the resistance of MRSA to the antibiotic fosfomycin and therefore validate FosB as a potential therapeutic drug target.

The fact that both BshA and FosB knockout strains of *S. aureus* Newman and USA300 JE2 have equally increased susceptibility to fosfomycin suggests that the thiol-dependent FosB detoxification pathway for fosfomycin is the primary resistance mechanism of the organism to the antibiotic. The MIC values for BSH null USA300 JE2 are reported to be 10−20 μg/mL.[33] Because the FosB null strains demonstrate a similar increase in sensitivity to fosfomycin, we can predict that the MIC value for fosfmycin in the FosB knockout USA300 JE2 is likely to be approximately the same (10−20 μg/mL). The reported maximal serum drug concentration (C_{max}) of fosfomycin following the standard 3 g oral dose is 22−32 mg/L within 2−2.5 h of treatment.[43] Thus, we might expect fosfomycin to be an effective treatment against multi-drug-resistant *S. aureus* if the FosB enzyme could be targeted therapeutically at least in a synergistic approach using multiple available antibiotics in addition to a FosB inhibitor.

■ CONCLUSION

We have obtained the first three-dimensional structures of FosB from *S. aureus*, the enzyme responsible for resistance of the pathogen to the antibiotic fosfomycin. $FosB^{Sa}$ catalyzes nucleophilic addition of BSH to the antibiotic and represents the sole fosfomycin inactivating pathway of the organism from the USA300 JE2 or Newman strains. The new structures provide insight into the functional role of the fosfomycin−

dx.doi.org/10.1021/bi4015852 | *Biochemistry* 2014, 53, 755−765

phosphonate binding loop of the enzyme. The loop probably functions as a door that opens and closes to allow the antibiotic to enter the active site of the enzyme. Once closed, the loop completes important structural features that bind and secure both cosubstrates. Contrary to previous results,[33] we have demonstrated that $FosB^{Sa}$ is inhibited by Zn^{2+}, as are all other reported VOC superfamily fosfomycin resistance enzymes. Given the similarity of the susceptibility of the BSH and FosB null strains of MRSA, we can predict the MIC values of FosB null MRSA to be 10−20 μg/mL, below the reported serum concentration of fosfomycin following the standard 3 g dose. Therefore, if $FosB^{Sa}$ could be targeted therpeutically, fosfomycin could very well serve as a synergystic treatment for pathogens like multi-drug-resistant strains of *S. aureus*.

■ ASSOCIATED CONTENT

Ⓢ Supporting Information

Additional protein figures and all X-ray fluorescence spectra. This material is available free of charge via the Internet at http://pubs.acs.org.

Accession Codes

The atomic coordinates and structure factors for structures reported in this work have been deposited in the Protein Data Bank as entries 4NAY, 4NAZ, 4ND0, 4NB1, and 4NB2.

■ AUTHOR INFORMATION

Corresponding Author

*Department of Biochemistry, Vanderbilt University Medical Center, Nashville, TN 37232. E-mail: r.armstrong@vanderbilt.edu. Phone: (615) 343-2920.

Funding

Supported by Grants R01 GM030910 to R.N.A., R01 AI069233 to E.P.S., T32 ES007028 to M.K.T. and M.E.K., and F32 GM093507 to P.D.C. from the National Institutes of Health.

Notes

The authors declare no competing financial interest.

■ ACKNOWLEDGMENTS

Use of the Advanced Photon Source, an Office of Science User Facility operated for the U.S. Department of Energy (DOE) Office of Science by Argonne National Laboratory, was supported by the U.S. DOE under Contract DE-AC02-06CH11357. Use of LS-CAT Sector 21 was supported by the Michigan Economic Development Corp. and the Michigan Technology Tri-Corridor (Grant 085P1000817). M.K.T. is grateful for the William N. Pearson Fellowship in Biochemistry provided by Vanderbilt University.

■ REFERENCES

(1) Fowler, V. G., Jr., Miro, J. M., Hoen, B., Cabell, C. H., Abrutyn, E., Rubinstein, E., Corey, G. R., Spelman, D., Bradley, S. F., Barsic, B., Pappas, P. A., Anstrom, K. J., Wray, D., Fortes, C. Q., Anguera, I., Athan, E., Jones, P., van der Meer, J. T., Elliott, T. S. J., Levine, D. P., and Bayer, A. S. (2005) *Staphylococcus aureus* endocarditis. A consequence of medical progress. *JAMA, J. Am. Med. Assoc. 293*, 3012−3021.

(2) Klevens, R. M., Morrison, M. A., Nadle, J., Petit, S., Gershrnan, K., Ray, S., Harrison, L. H., Lynfield, R., Dumyati, G., Townes, J. M., Craig, A. S., Zell, E. R., Fosheim, G. E., McDougal, L. K., Carey, R. B., and Fridkin, S. K. (2007) Invasive methicillin-resistant *Staphylococcus aureus* infections in the United States. *JAMA, J. Am. Med. Assoc. 298*, 1763−1771.

(3) Kuehnert, M. J., Kruszon-Moran, D., Hill, H. A., McQuillan, G., McAllister, S. K., Fosheim, G., McDougal, L. K., Chaitram, J., Jensen, B., Fridkin, S. K., Killgore, G., and Tenover, F. C. (2006) Prevalence of *Staphylococcus aureus* nasal colonization in the United States, 2001−2002. *J. Infect. Dis. 193*, 172−179.

(4) Lowy, F. D. (1998) *Staphylococcus aureus* infections. *N. Engl. J. Med. 339*, 520−532.

(5) Falagas, M. E., Giannopoulou, K. P., Kokolakis, G. N., and Rafailidis, P. I. (2008) Fosfomycin: Use beyond urinary tract and gastrointestinal infections. *Clin. Infect. Dis. 46*, 1069−1077.

(6) Falagas, M. E., Kastoris, A. C., Karageorgopoulos, D. E., and Rafailidis, P. I. (2009) Fosfomycin for the treatment of infections caused by multidrug-resistant non-fermenting Gram-negative bacilli: A systematic review of microbiological, animal and clinical studies. *Int. J. Antimicrob. Agents 34*, 111−120.

(7) Bernat, B. A., Laughlin, L. T., and Armstrong, R. N. (1997) Fosfomycin Resistance Protein (FosA) Is a Manganese Metalloglutathione Transferase Related to Glyoxalase I and the Extradiol Dioxygenases. *Biochemistry 36*, 3050−3055.

(8) Bernat, B. A., Laughlin, L. T., and Armstrong, R. N. (1999) Elucidation of a Monovalent Cation Dependence and Characterization of the Divalent Cation Binding Site of the Fosfomycin Resistance Protein (FosA). *Biochemistry 38*, 7462−7469.

(9) Arca, P., Hardisson, C., and Suarez, J. E. (1990) Purification of a glutathione S-transferase that mediates fosfomycin resistance in bacteria. *Antimicrob. Agents Chemother. 34*, 844−848.

(10) Arca, P., Rico, M., Brana, A. F., Villar, C. J., Hardisson, C., and Suarez, J. E. (1988) Formation of an adduct between fosfomycin and glutathione: A new mechanism of antibiotic resistance in bacteria. *Antimicrob. Agents Chemother. 32*, 1552−1556.

(11) Fillgrove, K. L., Pakhomova, S., Newcomer, M. E., and Armstrong, R. N. (2003) Mechanistic Diversity of Fosfomycin Resistance in Pathogenic Microorganisms. *J. Am. Chem. Soc. 125*, 15730−15731.

(12) Fillgrove, K. L., Pakhomova, S., Schaab, M. R., Newcomer, M. E., and Armstrong, R. N. (2007) Structure and Mechanism of the Genomically Encoded Fosfomycin Resistance Protein, FosX, from *Listeria monocytogenes*. *Biochemistry 46*, 8110−8120.

(13) Llaneza, J., Villar, C. J., Salas, J. A., Suarez, J. E., Mendoza, M. C., and Hardisson, C. (1985) Plasmid-mediated fosfomycin resistance is due to enzymic modification of the antibiotic. *Antimicrob. Agents Chemother. 28*, 163−164.

(14) Mendoza, C., Garcia, J. M., Llaneza, J., Mendez, F. J., Hardisson, C., and Ortiz, J. M. (1980) Plasmid-determined resistance to fosfomycin in *Serratia marcescens*. *Antimicrob. Agents Chemother. 18*, 215−219.

(15) Rife, C. L., Pharris, R. E., Newcomer, M. E., and Armstrong, R. N. (2002) Crystal Structure of a Genomically Encoded Fosfomycin Resistance Protein (FosA) at 1.19 Å Resolution by MAD Phasing Off the L-III Edge of Tl+. *J. Am. Chem. Soc. 124*, 11001−11003.

(16) Villar, C. J., Mendoza, M. C., and Hardisson, C. (1981) Characterization of two resistance plasmids from a clinical isolate of *Serratia marcescens*. *Microbios Lett. 18*, 87−95.

(17) Gaballa, A., Newton, G. L., Antelmann, H., Parsonage, D., Upton, H., Rawat, M., Claiborne, A., Fahey, R. C., and Helmann, J. D. (2010) Biosynthesis and functions of bacillithiol, a major low-molecular-weight thiol in bacilli. *Proc. Natl. Acad. Sci. U.S.A. 107*, 6482−6486.

(18) Cao, M., Bernat, B. A., Wang, Z., Armstrong, R. N., and Helmann, J. D. (2001) FosB, a cysteine-dependent fosfomycin resistance protein under the control of σW, an extracytoplasmic-function σ factor in *Bacillus subtilis*. *J. Bacteriol. 183*, 2380−2383.

(19) Lamers, A. P., Keithly, M. E., Kim, K., Cook, P. D., Stec, D. F., Hines, K. M., Sulikowski, G. A., and Armstrong, R. N. (2012) Synthesis of bacillithiol and the catalytic selectivity of FosB-type fosfomycin resistance proteins. *Org. Lett. 14*, 5207−5209.

(20) Newton, G. L., Rawat, M., La, C. J. J., Jothivasan, V. K., Budiarto, T., Hamilton, C. J., Claiborne, A., Helmann, J. D., and Fahey, R. C.

(2009) Bacillithiol is an antioxidant thiol produced in bacilli. *Nat. Chem. Biol. 5*, 625−627.
(21) Newton, G. L., Fahey, R. C., and Rawat, M. (2012) Detoxification of toxins by bacillithiol in *Staphylococcus aureus*. *Microbiology 158*, 1117−1126.
(22) Rajkarnikar, A., Strankman, A., Duran, S., Vargas, D., Roberts, A. A., Barretto, K., Upton, H., Hamilton, C. J., and Rawat, M. (2013) Analysis of mutants disrupted in bacillithiol metabolism in *Staphylococcus aureus*. *Biochem. Biophys. Res. Commun. 436*, 128−133.
(23) Otwinowski, Z., and Minor, W. (1997) Processing of X-ray diffraction data collected in oscillation mode. *Methods Enzymol. 276*, 307−326.
(24) Sheldrick, G. M. (2008) A short history of SHELX. *Acta Crystallogr. A64*, 112−122.
(25) McCoy, A. J., Grosse-Kunstleve, R. W., Adams, P. D., Winn, M. D., Storoni, L. C., and Read, R. J. (2007) Phaser crystallographic software. *J. Appl. Crystallogr. 40*, 658−674.
(26) Langer, G., Cohen, S. X., Lamzin, V. S., and Perrakis, A. (2008) Automated macromolecular model building for X-ray crystallography using ARP/wARP version 7. *Nat. Protoc. 3*, 1171−1179.
(27) Emsley, P., and Cowtan, K. (2004) Coot: Model-building tools for molecular graphics. *Acta Crystallogr. D60*, 2126−2132.
(28) Murshudov, G. N., Vagin, A. A., and Dodson, E. J. (1997) Refinement of macromolecular structures by the maximum-likelihood method. *Acta Crystallogr. D53*, 240−255.
(29) Pettersen, E. F., Goddard, T. D., Huang, C. C., Couch, G. S., Greenblatt, D. M., Meng, E. C., and Ferrin, T. E. (2004) UCSF Chimera: A visualization system for exploratory research and analysis. *J. Comput. Chem. 25*, 1605−1612.
(30) Rigsby, R. E., Fillgrove, K. L., Beihoffer, L. A., and Armstrong, R. N. (2005) Fosfomycin resistance proteins: A nexus of glutathione transferases and epoxide hydrolases in a metalloenzyme superfamily. *Methods Enzymol. 401*, 367−379.
(31) Thompson, M. K., Keithly, M. E., Harp, J., Cook, P. D., Jagessar, K. L., Sulikowski, G. A., and Armstrong, R. N. (2013) Structural and chemical aspects of resistance to the antibiotic fosfomycin conferred by FosB from *Bacillus cereus*. *Biochemistry 52*, 7350−7362.
(32) Armstrong, R. N. (2000) Mechanistic diversity in a metalloenzyme superfamily. *Biochemistry 39*, 13625−13632.
(33) Roberts, A. A., Sharma, S. V., Strankman, A. W., Duran, S. R., Rawat, M., and Hamilton, C. J. (2013) Mechanistic studies of FosB: A divalent-metal-dependent bacillithiol-S-transferase that mediates fosfomycin resistance in *Staphylococcus aureus*. *Biochem. J. 451*, 69−79.
(34) Finney, L. A., and O'Halloran, T. V. (2003) Transition Metal Speciation in the Cell: Insights from the Chemistry of Metal Ion Receptors. *Science 300*, 931−936.
(35) Kehl-Fie, T. E., Chitayat, S., Hood, M. I., Damo, S., Restrepo, N., Garcia, C., Munro, K. A., Chazin, W. J., and Skaar, E. P. (2011) Nutrient metal sequestration by calprotectin inhibits bacterial superoxide defense, enhancing neutrophil killing of *Staphylococcus aureus*. *Cell Host Microbe 10*, 158−164.
(36) Karavolos, M. H., Horsburgh, M. J., Ingham, E., and Foster, S. J. (2003) Role and regulation of the superoxide dismutases of *Staphylococcus aureus*. *Microbiology (Reading, U.K.) 149*, 2749−2758.
(37) Andreini, C., Banci, L., Bertini, I., and Rosato, A. (2006) Zinc through the Three Domains of Life. *J. Proteome Res. 5*, 3173−3178.
(38) Corbin, B. D., Seeley, E. H., Raab, A., Feldmann, J., Miller, M. R., Torres, V. J., Anderson, K. L., Dattilo, B. M., Dunman, P. M., Gerads, R., Caprioli, R. M., Nacken, W., Chazin, W. J., and Skaar, E. P. (2008) Metal Chelation and Inhibition of Bacterial Growth in Tissue Abscesses. *Science 319*, 962−965.
(39) McCormick, A., Heesemann, L., Wagener, J., Marcos, V., Hartl, D., Loeffler, J., Heesemann, J., and Ebel, F. (2010) NETs formed by human neutrophils inhibit growth of the pathogenic mold *Aspergillus fumigatus*. *Microbes Infect. 12*, 928−936.
(40) Urban, C. F., Ermert, D., Schmid, M., Abu-Abed, U., Goosmann, C., Nacken, W., Brinkmann, V., Jungblut, P. R., and Zychlinsky, A. (2009) Neutrophil extracellular traps contain calprotectin, a cytosolic protein complex involved in host defense against *Candida albicans*. *PLoS Pathog. 5*, No. e1000639.
(41) Horsburgh, M. J., Wharton, S. J., Cox, A. G., Ingham, E., Peacock, S., and Foster, S. J. (2002) MntR modulates expression of the PerR regulon and superoxide resistance in *Staphylococcus aureus* through control of manganese uptake. *Mol. Microbiol. 44*, 1269−1286.
(42) Lindsay, J. A., and Foster, S. J. (2001) zur: A Zn^{2+}-responsive regulatory element of *Staphylococcus aureus*. *Microbiology (Reading, U.K.) 147*, 1259−1266.
(43) Patel, S. S., Balfour, J. A., and Bryson, H. M. (1997) Fosfomycin tromethamine, a review of its antibacterial activity, pharmacokinetic properties and therapeutic efficacy as a single-dose oral treatment for acute uncomplicated lower urinary tract infections. *Drugs 53*, 637−656.